The Serra Pelada Au - Pd - Pt Deposit, Carajas, Brazil

Geochemistry, Mineralogy, and Zoning of Hydrothermal Alteration

The Serra Pelada Au – Pd– Pt Deposit, Carajás, Brazil: Geochemistry, Mineralogy and Zoning of Hydrothermal Alteration

Gabriel V. Berni[1], Christoph A. Heinrich[1,2], Lydia M. Lobato[3], Victor J. Wall[4], Carlos A. Rosière[3], Marcelo A. Freitas[4]

1 – Institute of Geochemistry and Petrology, Department of Earth Sciences, ETH Zürich, Clausiusstrasse, 25, NW F 82.1, 8092, Zürich, Switzerland

2 – Also at: Faculty of Mathematics and Natural Sciences, University of Zürich

3 – Centro de Pesquisa Manoel Teixeira da Costa, Universidade Federal de Minas Gerais, Av. Antônio Carlos, 6627, Belo Horizonte, Brazil

4 – Colossus Minerals Inc., The Exchange Tower, 130 King Street West, Suite 2500, Toronto, Ontario, Canada, M5X 1A9

Corresponding author: gabriel.berni@erdw.ethz.ch

Abstract

The Serra Pelada Au – Pd – Pt deposit is located within the Carajás Mineral Province, which also hosts the world class iron ore and iron-oxide hosted copper - gold deposits of the Amazon craton in Brazil. The unusual low-temperature hydrothermal mineralization at Serra Pelada is epigenetic, hosted by metasedimentary rocks of the Águas Claras Formation and structurally localized in the Serra Pelada overturned syncline. The ore bodies are controlled by the intersection of subvertical NE-trending fault zones with metasiltstones, mainly at the syncline's hinge, with minor ore occurrences at the upper and lower limb. Intense tropical weathering over the last 70Ma has completely overprinted the shallow ore in and near the flooded open pit, but primary hydrothermal features are preserved in deeper drill core delineating the remaining resource. Gold, platinum and palladium mineralization is associated with intense argillic alteration, hematite breccias and silicification, with the highest grade ore hosted by brecciated metasiltstones that are highly enriched in amorphous carbon. Distal alteration zones comprise a reducing and an oxidizing alteration front. The hydrothermal mineral paragenesis comprises kaolinite, quartz, sericite, amesite (Mg-rich Al-silicate), amorphous carbon, hematite, monazite, rutile, pyrite and a complex assemblage of Bi, Ag, Pb, Cu, Co, Ni, Pt, Pd and Au bearing, chalcogenide (S, Se) and arsenide (As, Sb) minerals. Major element changes during hydrothermal alteration include C and Mg addition, K depletion, localized silica loss and silicification with notable introduction of trace elements including LREE, Bi, Pb, U, V, Cu, Co, Ni and As. The hydrothermal alteration and the element association of the Serra Pelada deposit show geochemical similarities with unconformity-related uranium deposits, which may also be enriched in Au, Pd and Pt and were formed by mixing of fluids that interacted with a highly oxidized cover sequence and highly reduced rock packages in structures of brittle-ductile strain.

Introduction

The Serra Pelada Au – Pd – Pt deposit is located within the Itacaiúnas Belt, in the northern part of the Carajás Mineral Province and near the eastern edge of the Amazon craton in Brazil. The Itacaiúnas Belt comprises an Archean granite – gneiss basement and two metavolcanosedimentary sequences, the Itacaiúnas Supergroup and the Andorinhas Supergroup, which are overlain by two metasedimentary sequences. A set of granitic and mafic/ultramafic intrusions from Archean to Proterozoic ages also occurs in the province. Well known for the giant iron mines, the Carajás Mineral Province also hosts big (<300 Mt) iron-oxide hosted copper gold deposits (IOCG; e.g., Cristalino, Salobo, Igarapé-Bahia, Sossego), as well as some Au, Ni and Mn deposits (Grainger et al., 2008).

The Serra Pelada deposit was discovered in the early 1980´s, with over 80,000 artisanal miners working in a 400 by 300 meters open pit during the peak of activities in the following years. Site of the largest gold rush in South America, the deposit has become world famous by its spectacular metal concentration at near surface (e.g., drill hole FD-32 at 54.5-55.0 m containing 132,000 ppm Au, 11,000 ppm Pd and 359 ppm Pt; Cabral et al., 2002), containing gold as coarse-grained aggregates and nuggets up to 50 kg. An estimated production of 32.6 tons of Au was manually extracted from the open pit, which collapsed and flooded in 1984 (Meireles and Silva, 1988).

Two styles of ore are present in the Serra Pelada deposit: (1) The near-surface, bonanza style mineralization which formed the nuggets and wire-shaped particles of black palladian gold ("ouro preto"; Cabral et al. 2002, 2011); (2) The deep-seated mineralization, as the focus of this study which also hosts high metal concentrations (e.g., drill hole SPD099 at 239.95-242.30 m containing 4630 ppm Au, 1730 ppm Pd, 1600 ppm Pt; Colossus Minerals Inc., 2011) but is characterized by a sulfide-selenide-arsenide mineralogy.

First sub-surface exploration took place during the late 1980´s and early 1990´s, managed by VALE (formerly Companhia Vale do Rio Doce – CVRD). In 2007, the mining license was transferred to the mining cooperative of artisanal miners of Serra Pelada (COOMIGASP). A joint venture with the Canadian company Colossus Minerals Inc. started a new evaluation of the deposit in 2009, allowing access to fresh drill core samples (Wall et al., 2009).

Published work on the Serra Pelada area includes geological descriptions of the mine sequence (Jorge João et al., 1982; Meireles et al., 1982; Meireles and Silva, 1988; Tallarico et al., 2000), the ore geochemistry (Moroni

et al., 1999, 2001; Grainger et al., 2002), and the mineralogy and age dating with a main focus on the near-surface bonanza ore (Cabral et al., 2002, 2011).

Genetic models include an intrusion-related model (Tallarico et al., 2000) and Grainger et al. (2002) described the hydrothermal alteration within the ore zone and suggested a distal, low-temperature variant in the broad genetic group of iron-oxide copper-gold deposits of the Carajás Mineral Province. The hydrothermal process is thought to have occurred during Paleoproterozoic times, based on U-Pb ages of monazite intergrown with primary gold and PGE minerals (1861 ± 45 Ma – SHRIMP $^{208}Pb/^{232}Th$, Grainger et al., 2002). Cabral et al. (2011) dated a Mn-Ba oxide aggregate intergrown with palladiferous gold and Pd-Pt minerals within the bonanza ore and proposed a Late Cretaceous (75 ± 6 Ma; $^{40}Ar/^{39}Ar$) overprint of the Paleoproterozoic mineralization.

In previous studies, the deep weathering has limited the interpretation of primary features of hydrothermal alteration and mineralization, which is now more accessible by the recent drilling campaign. The present paper aims at characterizing the ductile to brittle deformation history of fresh ores and host rocks and their hydrothermal alteration in relation to primary variations in sedimentary rock composition, in preparation for more detailed studies of the primary ore mineralogy and the fluid-compositional evolution of the deposit based on fluid inclusions.

Regional Setting

The basement assemblage of the Itacaiúnas Belt (Fig. 1) consists of granite – gneiss terrains known as the Pium Complex (3002 ± 14 Ma; Pidgeon et al., 2000) and Xingu Complex (2,859 ± 2 Ma; Machado et al., 1991). Overlying supracrustal rocks are related to two different metavolcanosedimentary sequences. The older Andorinhas Supergroup is represented in the area of Figure 1 by the Rio Novo Group (ca. 2.9 Ga; Avelar et al., 1999; Villas and Santos, 2001) and consists of mafic to ultramafic schists with minor felsic rocks and banded iron formations (BIF). The younger Itacaiúnas Supergroup (ca. 2.76 Ga; Machado et al., 1991) is dominated by mafic metavolcanic rocks and BIF.

Two metasedimentary units unconformably overlie the metavolcanosedimentary sequences: (1) The Águas Claras Formation (hosting the Serra Pelada Au – Pd – Pt deposit) is composed of metasandstones and metasiltstones deposited in fluvial to marine environments during late Archean to lower Paleoproterozoic times (Nogueira et al., 1995). It unconformably overlies the Itacaiúnas Supergroup in the western and the Andorinhas Supergroup in the eastern portion of the area shown in Figure 1; (2) The Caninana unit (ca. 2.0 Ga; Prado-

Pereira, 2009) is also unconformably overlying the Itacaiúnas Supergroup and is composed of metasandstones and metaconglomerates deposited in a fluvial environment but its relationship with the Águas Claras Formation is yet to be established.

Intrusive rocks include the Luanga mafic/ultramafic complex (2,763 ± 6 Ma; Machado et al., 1991), syntectonic calc-alkaline granitoids and diorite bodies of the Plaquê Suite (ca. 2.74 Ga; Barros et al., 2000) and granites of the Estrela Complex (ca. 2.57 Ga; Machado et al., 1991). These older intrusions only cut the metavolcanosedimentary sequences and their basement, and are pervasively deformed. Anorogenic granitoids, mostly large alkaline A-type granite intrusions such as the Cigano and Central Carajás plutons (ca. 1.88 Ga; Machado et al., 1991), intrude all former rock units including the Águas Claras Formation. The metavolcanosedimentary and metasedimentary rocks of the Itacaiúnas Belt forms a set of WNW- and WSW-trending folds that locally progress to axial-plane thrust faults (Rosière et al., 2005), notably the Carajás and Cinzento strike-slip systems (Fig. 1). Pinheiro and Holdsworth (2000) interpret these faults as late Archean in age, reactivated in the Paleoproterozoic before being truncated by the anorogenic granites. The last major tectonic structure shown in Figure 1 is the frontal thrust of the Araguaia Fold Belt over the eastern border of the Amazon craton (Braziliano or Pan-African event, ca. 600 Ma; Almeida et al., 1981).

Geology of the Serra Pelada Au – Pd – Pt Deposit

Stratigraphy

The Serra Pelada Au – Pd – Pt deposit is hosted by the Águas Claras Formation, which unconformably overlies the Rio Novo Group (Tallarico et al., 2000; Grainger et al., 2002) in the northeastern portion of the Itacaiúnas Belt (Fig. 2). Here, the Rio Novo Group consists of mafic and ultramafic schists, BIF and minor felsic rocks (Tallarico et al., 2000). It is intruded by the Luanga mafic/ultramafic complex (U-Pb 2,763 ± 6 Ma; Machado et al., 1991) and by the Formiga Granite (uncertain age), which hosts some Au mineralization (Grainger et al, 2002).

In the Serra Pelada area, the Águas Claras Formation is formed by alternating metasandstone and metasiltstone units. The lower portions of the sequence outcrop at the Elefanto syncline and consist of basal metasandstones with polymictic conglomerate layers and laminated carbonaceous and red metasiltstones. The upper part of the sequence outcrops at the Serra Pelada syncline and Cedro anticline and is composed by metasandstones, dolomitic metasandstones with layers of metasiltstone and metaconglomerates, undifferentiated gray metasiltstones and red metasiltstone and an upper metasandstone sequence (Fig. 2).

The mine sequence at the Serra Pelada deposit (Fig. 3) overlies the mafic and ultramafic schists of the Rio Novo group (Fig. 4A) and consists of the following rock types, stratigraphically from bottom to top in the lower limb of the Serra Pelada syncline, as shown in Figures 4B to 4F:

Dolomitic sandstone (unit 1): Comprises impure fine- to coarse-grained sandstones cemented by fine-grained dolomite (Fig. 4B), and minor interlayers of mono- and polymictic conglomerates (Fig. 4C) with clasts of rounded quartz and minor fragments of BIF within a sandy and dolomitic matrix. This unit is weathered to pure friable sand near the surface and locally down to 300 m depth.

Gray metasiltstone (base of unit 2): Made of a thin, laminated metasiltstone composed of quartz, fine-grained muscovite (sericite), organic matter <0.1 wt % C_{total}) and rare pyrite (Fig. 4D, E). In the Serra Pelada syncline this rock forms a continuous 15-20 m thick layer at the base of the red metasiltstone. This lithology hosts the bulk of the precious-metal resource of the Serra Pelada deposit (Grainger et al., 2002).

Red metasiltstone (stratigraphic top of unit 2): Composed of centimeter-scale pink layers of fine sandstone and millimeter-thin laminar darker red pelitic layers (Fig. 4F). The mineralogy comprises muscovite, kaolinite, quartz, hematite and goethite (in decreasing abundance, Moroni et al., 2001). The rock shows well preserved sedimentary structures such as ripple marks and graded beds with coarse-grained bottom foresets (e.g. Fig 4F, steep structure). A weakly-schistose texture defined by a weak grano- to nematoblastic alignment of phyllosilicate minerals, hydrated Fe-oxide minerals and quartz within discrete zones, indicates the effects of low-grade metamorphism. Mineral assemblages within these minor zones include only locally developed muscovite (Grainger, 2003).

Intrusive rocks: Diorite bodies of uncertain age intruded the Rio Novo Group as well as the metasediments of the Águas Claras Formation. Tallarico et al. (2000) described the contact metamorphism associated with the diorite intrusion SW of the deposit (Fig. 3A), where the occurrence of actinolite + calcite and the local association of diopside indicate a minimum temperature of 550°C for the peak metamorphic conditions (dolomite + quartz + H_2O = actinolite + calcite + CO_2). Diorites, all sedimentary and earlier magmatic rocks were subsequently deformed and metamorphosed under lower greenschist facies (Grainger et al., 2002).

Structural Setting

Textures in the metasedimentary rocks of the Águas Claras Formation near Serra Pelada record two shortening deformation events (D_1 and D_2). The north-northwest verging D_1 event was related to regional-scale, tight and

asymmetrical NE-trending F_1 folds, mapped as the Serra Pelada and Elefanto synclines (Grainger et al., 2002) and the Cedro anticline (Berni, 2009). All three regional-scale folds plunge to SW. The Elefanto syncline and the Cedro anticline have moderately-dipping limbs (45-60º) and axis plunge (30-40º), whereas the Serra Pelada Syncline has shallow-dipping limbs (15-30º) and a gently plunging axis (15-20º). Progressive folding led to axial-plane thrust faults, possibly with associated oblique movement, which resulted in a stacking of the regional-scale F_1 folds such as the Serra Pelada and the Elefanto synclines (Fig. 2). The D_2 event is related to a low-strain deformation phase, with associated NE-trending subvertical faults and the development of a local crenulation cleavage and centimeter-scale folds. Later NW-trending faults offset all former structures and control the emplacement of Jurassic gabbro dikes (Tallarico et al., 2000).

The diorite intrusion pre-dates S_1 foliation and is the oldest intrusion in the area. The intrusion of the Cigano A-type granite (U-Pb age of 1.88 Ga; Machado et al., 1991) and a north-northwest-trending gabbro dike (Jurassic Rb-Sr age of 198 Ma; Meireles et al., 1982) postdate the S_1 metamorphic foliation.

The Serra Pelada deposit is localized in the homonymous syncline, but ore formation clearly postdates the D_1 event that formed this reclined fold (Grainger et al., 2002). The Serra Pelada syncline has a fold closure of semi-cylindrical geometry, showing little or no apical thickening. Later structures related with the D_2 event control the location of mineralization (Fig. 5A). These are subvertical NE-trending fault zones associated with a non-penetrative crenulation cleavage and small-scale open folds, which overprint the gently dipping axial-plane foliation (Fig.4E).

Ore grade distribution based on 3D modeling of drilling assays from the Serra Pelada deposit reflects this structural control on the large scale, defining two ore zones (Fig. 5B): (1) The Main Zone, located at the syncline's hinge and hosted by hydrothermally altered gray and red metasiltstones, with minor occurrences hosted by the dolomitic sandstones. It is subvertical and grossly tabular in shape, with approximately 100 m in height, a horizontal width up to 40m, at least 900m length extending from the open pit down along the gently plunging axis of the syncline towards SW. The main high-grade ore shoots (> 50 ppm Au) are narrow, rod-shaped, NE-trending and plunge gently to SW. (2) The Limb zones are located about 150-200 m west of the fold hinge mainly at the lower limb and locally at the upper limb of the syncline. Mineralization is hosted mainly by hydrothermally altered gray metasiltstone and is controlled by the intersection of another fault zone parallel to the main zone at the lower limb of the syncline which resulted in a flat-lying ore shoot, having 10-15 m in vertical thickness, and approximately 50 m in width.

Analytical Methods and Sample Material

Samples of the least-altered siltstones and of altered and mineralized rocks were selected from 28 different drill cores within the deposit plus samples from two high-grade intervals from the exploration program of Colossus Minerals Inc. Description of the drill hole depth, individual methods, detection limits, and quality control data are listed in Table 1 of the digital repository. Whole-rock analyses of major, trace and noble metals (Au, Pt and Pd) were carried out by Genalysis Intertec Laboratory Services (Perth, Australia) on 349 samples. Drill core samples were pulverized, homogenized and aliquots of 50 g were dissolved in sodium peroxide fusion and hydrochloric acid. Major elements, plus B, Cu, Sc, V, Zn, S, Co and Cr were analyzed by inductively coupled plasma optical emission spectrometry (ICP-OES) and other trace elements and REE by inductively coupled plasma mass spectrometry (ICP-MS). Precious metal (Au-Pt-Pd) analyses where made by fire assay (25 g) prior to LA-ICPMS.

In order to have a better understanding of the bulk rock data obtained from core intersections without close spatial control, we quantified bulk-rock ratios of major element from small-scale variations of sedimentary layers, mm-scale barren argillic halos, quartz-kaolinite veinlets and some massive carbon- and kaolinite-rich argillic rocks by LA-ICPMS analysis of polished slabs of these very fine-grained rocks. We used the Excimer LA-ICPMS at ETH Zürich (Günther et al., 1997) and large shallow ablation pits of 110µm diameter, which yielded quite homogeneous signals allowing evaluation of averaged major element ratios in the rock. Analytical and standardization procedures were performed using the NIST SRM 610 as an external reference material according to Heinrich et al. (2003). Element ratios were calculated using the SILLS software (Guillong et al., 2008). Table 2 (see digital repository item) reports the core-scale bulk-rock analyses and small-scale LA-ICPMS ratios for the selected samples.

For detailed mineralogy studies we used a JEOL JSM - 6390LA scanning electron microscope (SEM) attached to a Thermo Scientific UltraDry EDS detector at ETH Zürich.

Hydrothermal Alteration and Mineralization

The mineralization at Serra Pelada is a fracture-controlled system on all scales. Two contrasting distal hydrothermal alteration comprises chlorite / carbon alteration and wide spread hematite alteration in metasediments and metavolcanic rocks at different location within of the deposit vicinity (Fig. 3B). The main mineralized zone is located at the hinge of the fold and comprises carbon-rich argillic alteration, silicification and hematite breccias (Fig. 6).

Distal alteration types

Chlorite-carbon alteration: the chlorite-carbon alteration is the most widespread alteration feature within the metasiltstone sequence. It transgressively overprints the red metasiltstone sequence along the contact between the dolomitic sandstone and the gray metasiltstone, up to 350 m away from the ore zone (Fig 3B). The alteration features are readily recognized by the precipitation of chlorite and carbon along fractures and the compositional layering of the red metasiltstone (Fig. 7A). Carbon precipitation is visible within veins that cross-cut the already chlorite altered metasiltstone (Fig. 7B), or along S_2 crenulation planes (Fig. 7C and 4E). The alteration replaces low-grade metamorphic muscovite by chlorite along fractures and their halos with associated carbon addition, which turns the red metasiltstone into a green-grayish colored rock. The alteration assemblage comprises chlorite + amorphous carbon + muscovite + quartz with minor pyrite, chalcopyrite and goethite (pseudomorphs after pyrite or magnetite).

Hematite alteration: this is a patchy alteration feature which is observed up to 250 m away from the ore zone. In restricted areas of subvertical fracturing, dolomitic sandstone is changed to a hematite dusted recrystallized marble with numerous dissolution vugs (Fig. 3B,7D). These vugs are lined by cm-sized euhedral crystals of co-precipitating quartz, hematite - dusted dolomite (Fig. 7E) and late calcite. Growth zones within the quartz and dolomite crystals include abundant hematite, with minor pyrite, chalcopyrite and carrollite-fletcherite ($Cu(Ni,Co)_2S_4$). Bulk (110 µm ablation pits) LA-ICPMS analyses of these growth zones yield concentrations of 100's ppb of Pt, evidencing the distal relationship of this alteration with the ore mineralization. Within the red metasiltstone sequence, comparable hematite alteration is restricted to a few quartz-hematite veins crosscutting the earlier S_1 foliation. Regionally, quartz-hematite breccias are observed near the main fault zones hosted by metasediments or by the metavolcanic basement up to 6 km from the deposit.

Hydrothermal Alteration of the Mineralized Zones

Argillic alteration overprints carbon-enriched metasiltstones (> 10 wt.% C_{total}) and is most closely associated with the bulk of the Au-Pt-Pd resource within the deposit. It can be subdivided in three subtypes, the carbon-, kaolinite- and hematite-rich argillic zones (Fig 6). Most of the ore occurs with carbon-rich argillic alteration, where the ore texture varies from a coherent carbon-enriched metasiltstone with stylolitic quartz – kaolinite veins (Fig. 8A) to high-grade friable breccias with metasiltstones fragments within a carbon – quartz – kaolinite matrix (Fig. 8B). The stylolitic veins are mostly associated with flat fractures, consistent with subhorizontal shortening associated to the D_2 deformation event. Carbon-poor zones of intense kaolinite-rich

(Fig. 8C) and hematite-rich argillic alteration (Fig. 8D) occur as thin discontinuous bodies between the main carbon-rich argillic ore (Fig. 6) and often present breccia textures. It replaces the metamorphic muscovite by kaolinite, locally associated with coarse-grained hydrothermal muscovite and locally amesite. Gold occurs as aggregates of fine pureness (< 2 wt.% Ag) and fischesserite (Ag_3AuSe_2), as isolated grains within the matrix, or included in quartz, monazite, hematite sulfides and selenides. Palladium minerals are arsenopalladinite ($Pd_8(As,Sb)_3$), isomertieite ($Pd_{11}Sb_2As_2$) and mertieite ($Pd_{11}(Sb,As)_4$). Palladseite ($Pd_{17}Se_{15}$) was also identified by Grainger (2003). Platinum phases are fine grained braggite (Pt,Pd,Ni)S, Sperrylite ($PtAs_2$), sudovikosvite ($PtSe_2$) and isoferroplatinum (Pt_3Fe). Palladian gold was reported by Cabral et al. (2002), containing inclusions of Pd-arsenides, isomertieite, palladseite, sudovikosvite and a Pt-Pd-Se phase, but this texturally overgrowing alloy was found only within the oxidized ore within and just below the former open pit mine. Other accessory minerals within the primary hydrothermal ore comprise pyrite, chalcopyrite, covellite, selenian covellite, Ag-Cu-Fe sulfide, carrollite-fletcherite ($Cu(Co,Ni)_2S_4$), galena, barite, anhydrite, rutile, clausthalite (PbSe), naumannite (Ag_2Se) and litochlebite ($Ag_3PbBi_4Se_8$). Detailed investigation of this complex mineralogy is in progress. Barren argillic alteration extends to the inner hinge of the Serra Pelada syncline and consists of zones of carbon removal (bleaching) along S_2 crenulation planes, with associated sericite, kaolinite, quartz, hematite and/or rare pyrite (Fig. 8E).

Siliceous alteration envelops the argillic altered rocks mainly at the upper and lower limb of the Serra Pelada syncline and locally at the inner hinge (Fig. 6). The dolomitic sandstones in the outer part of the fold hinge and the metasiltstones at the inner hinge are changed to fine- to coarse-grained quartz with minor hematite and pyrite. Mineralization is sub-economic (mostly sub-ppm Au grades) and locally higher grades are normally restricted to silicified gray metasiltstone (Grainger et al., 2002). Silicification includes early crack-seal veins and even recrystallized veins that were folded by the metamorphic S_1 deformation (Fig. 8F). The greater part of silicification around the orebody does not show any S_1-related structure, indicating that it occurred during ore formation. It is formed by fine grained massive to coarse and locally vuggy quartz, with contemporaneous hematite and carbon veinlets (Fig. 8G), suggesting that reduced and oxidizing alteration fronts formed at overlapping times later in the deformation history. The vugs are patchy dissolution features, rather than fracture openings. They are typically lined by fine-grained or globular hematite that is overgrown by clear euhedral quartz crystals (Fig. 8H), indicating local silica dissolution and re-precipitation. The mineral assemblage is quartz with minor fine-grained muscovite, kaolinite, hematite, pyrite and rare chalcopyrite. The siliceous alteration corresponds to the jasperoid alteration described by Tallarico et al. (2000) and Grainger et al. (2002), terminology defined as fine-grained to cryptocrystalline silica replacement of carbonate rocks by

Neuendorf et al. (2005). At Serra Pelada, silicification replaces both metasiltstone and dolomitic sandstone, and therefore the more general term is used here.

Hematite breccias locally with economic ore grades occur in the Limb Zone, with a few low grade occurrences also in the Main Zone of the deposit (Fig. 6C). This breccia is made up of angular fragments of metasiltstone and fine grained silica within a goethite matrix (weathered hematite/pyrite). In the Limb Zone, the breccias are matrix supported and contain a greater proportion of metasiltstone fragments, whereas similar breccias in the main zone are clast supported, with predominantly siliceous fragments. These breccias host high-grade Pd-Pt mineralization up to hundreds ppm Pt+Pd, with particularly high Pt+Pd/Au ratios.

Geochemistry of Hydrothermal Alteration

Bulk-rock geochemistry

Figures 9A and B show the bulk concentration ranges of typically immobile elements such as Al, Ti and Zr for least altered host rocks and variably mineralized samples. Within the range of the primary sedimentary variations, those elements are kept in the same proportions in the protolith and altered rocks, and therefore can be used to assess significant element changes during the hydrothermal alteration, at least in a qualitative way. Major element variations observed between the least altered metasedimentary rocks and the hydrothermally altered rocks within the ore zone can be explained by variable additions of C and Mg and loss of K with localized silica addition and loss (Fig. 9).

Some of the *kaolinite-rich argillic* samples show elevated concentrations of residual immobile elements (yellow triangles in Fig. 9A and 9B), indicating net mass removal of K and also some Si. This is shown in Figure 9C, where the K/Al values within samples of the kaolinite-rich argillic reach much lower values and decrease faster (in respect to K/Si) than those in carbon-rich argillic samples. The Si/Al ratio slightly increases or the ratio is kept at a nearly constant value, in respect to Si/K values, implying smaller silica addition associated with this type (Fig. 9D).

In the *carbon-rich argillic* alteration and many other ore-related rocks, the concentrations of Al, Ti and Zr are lowered in near-constant proportions compared to the least altered siltstones (Figs. 9A, 9B), requiring massive dilution by addition of C, Si and Mg with localized silica loss (Fig. 9D). Most of the carbon-rich argillic samples show a similar trend as observed within the kaolinite-rich argillic samples, with a Si/K ratios increase and nearly constant Si/Al implying K loss. The same trend is also visible within small-scale barren argillic

alteration haloes (orange crosses in Figs. 9D). For some of the carbon-rich argillic rocks, the values of Si/K increase together with Si/Al within the carbon-rich argillic rocks, implying a Si input, in total exceeding the mass loss by K leaching in this alteration type. A few samples show smaller Si/Al values than the least altered metasedimentary rocks, suggesting localized Si-loss. (Fig. 9D).

Mg enrichment is also associated with many kaolinite-rich and some of the carbon-rich argillic samples, as shown in Figure 9E, where the higher increase of Mg/Al values compared to Mg/K cannot be explained by K loss only (cf. two dashed arrows in Fig. 9E).

Structural relations indicate that this intense carbon addition occurred at the same time as the distal chlorite-carbon alteration (Figs. 4E and 7B), raising the carbon content from 0.1 wt.% C_{total} in the least altered gray siltstone up to 10% wt.% C_{total} within the carbon-rich argillic alteration. The association of the most carbon-enriched zone with S_2 crenulations, fracturing and brecciation indicates that carbon addition was a hydrothermal process associated with ore formation. There is no direct correlation of Au+Pd+Pt grades with carbon content, but the highest grades in primary ore consistently occur in samples with carbon content higher than 3 wt.% (Fig. 10A).

The *siliceous alteration* zone is dominated by dilution of Al, Ti and Zr by quartz, requiring strong Si addition in most samples of massive granular and vuggy quartz. The low Zr and Ti concentrations in these rocks argue against a primary origin of silica-rich rocks as sandstone lenses, in which detrital rutile and zircon should be enriched compared to clay minerals (i.e., Al) in shales. Note that the high K/Al > 0.4 (at very low K, Al) reported in Figure 9C for some of the most siliceous samples must be analytical artifacts due to incomplete dissolution of minor clay minerals, rather than indicating the presence of K-feldspar.

Precious metals and related trace-elements including Bi, Pb, U, Se, Te, As, Sb and V are highly enriched compared to the least altered metasediments and broadly correlate with Au + Pt + Pd ore grades (Fig. 10B-F), in contrast to the dilution trends exhibited by the immobile elements. This is consistent with the textural evidence that monazite, clausthalite and Bi-V oxides are commonly being intergrown with Au, Pt and Pd selenides, Sb and As bearing minerals. Significant enrichment of all these ore-related trace elements is also largely associated with elevated carbon contents. Geochemical analyses for Rh and Ir carried out in a few mineralized samples (carbon-rich argillic rocks only – Figs. 10G and H) show good correlation for Rh with Au+Pt+Pd grades and a more broad correlation for Ir. All altered rocks also display highly enriched values of LREE (in monazite) and elevated Cu, Co and Ni.

Au-Pt-Pd Distribution within Major Alteration Types

From the hydrothermal alteration we can therefore distinguish two main ore types; the carbon-rich argillic ore (80-85% of the ore tonnage) and the kaolinite-rich argillic ore (5-10%). Other ore types are minor and have a more variable grade distribution, including the hematite breccia restricted to the lower Limb Zone (~5% of the resource) and a few occurrences within siliceous alteration and hematite-rich argillic rocks (< 5 %).

The Au – Pd – Pt distribution is broadly correlated, with Au >Pd ≥ Pt (Moroni et al., 2001) but with variable ore-metal ratios associated with the different alteration types. Figure 11 shows plots of Au vs. Pt+Pd and Pt vs. Pd for the different alteration types within the deposit. Samples of the high-grade bonanza ore that was mined are represented by samples from the old pit including data published by Cabral et al. (2002). Lines of constant element ratio are displayed for reference.

For the highest grades, Au and Pd + Pt are clearly correlated in all argillic altered rocks, showing that the exceptional element association and their extreme degree of enrichment are related with each other. However, very high Au or Pt + Pd grades also occur with low to modest grades of the other metal, in all types of alteration.

The ore grade within the carbon- and the kaolinite-rich argillic rocks is extremely variable, ranging from weight percent's down to less than a ppm in the low-grade samples. Generally Au grade is higher than Pt + Pd (Fig. 11A, 11B), except for some samples with high Pt+Pd to Au ratios. The majority of samples of the deep seated mineralization is somewhat enriched in Au relative to Pt+Pd, but samples from the bonanza ore show the highest Au to Pt + Pd ratios. Likewise, the Pt to Pd ratios within the carbon- and argillic-rich ores are relatively constant around 1 for the deep sited mineralization, while Pd can be enriched relative to Pt up 12x in the bonanza ore samples (Fig. 11C,11D).

The hematite-argillic and the siliceous alteration are generally poor in metal contents, with a few high-grade samples. The Au to Pt+Pd ratios are extremely variable within both types of alteration (Fig. 11E,11 F). The same differences observed between the bonanza ore and the deep mineralization are also evident with the hematite-rich argillic ore (Fig. 11G). As expected since siliceous-rich rocks are less susceptible to weathering, the same is not observed in the siliceous samples within the pit (Fig. 11H).

Discussion

Late Cretaceous bonanza style upgrading at Serra Pelada

In a recent paper, Cabral et al. (2011) interpret the genesis of the bonanza-style ore, with coarse wires of palladian gold (e.g. FD 0032), to be a product of a Late Cretaceous hydrothermal event (75 ± 6 Ma) and implied that such a late hydrothermal event was the main process that generated the spectacular precious metal endowment of this unusual deposit. Their conclusion is based on ^{40}Ar-^{39}Ar dating of a Mn-Ba oxide aggregate from a thoroughly oxidized high-grade ore sample, which the authors consider to be coeval with hydrothermal quartz and hematite of the type we describe in the present paper, rather than being a product of the long lasting lateritization of the Carajás region that started around the same time (~72 Ma; Vasconcelos et al., 1994). Additional geochemical arguments for a Cretaceous hydrothermal process are (1) iridium concentrations were supposedly depleted in the bonanza-ore style mineralization compared to the primary ores, requiring a hydrothermal overprint because Ir is extremely immobile in surface waters (Anbar et al., 1996 in Cabral et al., 2011); and (2) the supposed Bi-rich affinity of the deep-seated mineralization compared to As, Sb, Se and Hg enrichment of the bonanza style.

Our results show that none of these hydrothermal features described by Cabral et al. (2011) are restricted to the fully-oxidized bonanza-grade ore, and that they were generated by the hydrothermal processes that formed the primary high-grade ore at depth. Cavity-filling tabular hematite is widely and intimately associated with euhedral quartz in the periphery of the primary carbonaceous ore (e.g. Figs. 7D and 7E). Both are indeed hydrothermal, but unlikely to be coeval with the Cretaceous Mn-Ba oxides dated by Cabral et al. (2011). The Au-Pt-Pd concentrations show a good correlation with Bi, but the association with As, Sb, Te and Se is equally pronounced in the primary ore and not a geochemical feature restricted to the oxidized bonanza ore (Fig. 10F). Clearly hydrothermal quartz - kaolinite veins (Fig. 8A) and other argillic-altered rocks contain selenides, Sb-arsenides and sulfides as primary minerals, and in the bonanza ore mineralization these minerals are found as relict inclusions in palladian gold. Selective Ir depletion would be a valid argument against an origin of the bonanza ore by weathering, but the argumentation that the deep-seated mineralization is strongly enriched in Ir is not clear. Ir analyses presented in this contribution and also by Grainger, 2003 show that the concentration of Ir is quite variable within high-grade Au-Pd-Pt samples of the deep-seated mineralization and samples of high-grade Au+Pd+Pt (< 100 ppm) also show low Ir concentrations (Fig. 10G).

Even though the bonanza-style ore contains the spectacular gold nuggets and extremely high-grade ore that triggered the discovery of the deposit and the gold rush, we conclude that this overprint was not the main process that generated this unusual ore deposit. Deep seated high-grade ore dominated by Bi-Se-Te-As-Sb-bearing Pt and Pd minerals already produced spectacular ore grades up to 5000 ppm Au+Pt+Pd, with a metal enrichment of 7 orders of magnitude compared with ordinary crustal rocks. Mn – Fe – oxide rich bonanza ore formation involved a further enrichment by at most 1 order of magnitude compared to the primary, dominantly carbonaceous ore (Fig. 11). This emphasizes that exploration criteria should be focused on the primary mineralization features at regional to local scale, which we will further discuss in the following sections.

Timing of hydrothermal Au – Pd – Pt mineralization with respect to regional deformation history

The alteration zoning around the Serra Pelada syncline's hinge implies that this pre-mineralization structure, caused by regional deformation and metamorphism (D_1) in the late Archean, was an important factor in the ground preparation for localizing the orebody. However, mineralization occurred later during tectonic reactivation (D_2) in Paleoproterozoic times. Grainger et al. (2008) dated hydrothermal monazite intergrown with Au and Pt-Pd minerals (U-Pb SHRIMP age of 1861 ± 45 Ma) within the Serra Pelada deposit, indicating that this is the most likely age of primary low-temperature hydrothermal Au-Pd-Pt enrichment to grades of thousands of ppm of each of the precious metals. We suggest that the D_2 event was associated with minor regional deformation in the Paleoproterozoic, well after major pervasive deformation of the Carajás block in the late Archean. Low-strain, mostly brittle deformation locally reactivated the main E-W fault systems of Archean age, and developed the main NE fault zones controlling the Serra Pelada mineralization. Temporal overlap of the interpreted age of mineralization with the emplacement of Paleoproterozoic alkaline granitoids (1883 ± 2 Ma - U-Pb on zircon by SHRIMP, Machado et al. 1991) indicates a common, anorogenic thermotectonic event in the region, but does not necessarily prove a genetic link of hydrothermal ore formation to the distal granitoid plutons and any magmatic fluids they may have generated, as tentatively implied by Grainger et al. (2008).

Hydrothermal alteration and mineralization at Serra Pelada: variant of an unconformity-related U deposits

Textural and geochemical data presented in this paper demonstrate a hydrothermal, epigenetic origin of the primary high-grade Au, Pd and Pt mineralization at Serra Pelada. Deep-reaching carbonate dissolution in the dolomite-cemented sandstones and supergene modification of the primary ore mineralogy to palladian gold alloys and Mn-Fe oxy-hydroxides has largely overprinted the primary hydrothermal alteration and high-grade

mineralization, which therefore has been missed or rejected in earlier studies. We have shown here that quartz, hematite and kaolinite associated with the primary sulfide and selenide mineralization at the Serra Pelada Au – Pd – Pt deposit (e.g. Fig. 8A) are not a product of weathering. The orebody geometry and associated argillic alteration of the outer portions of the fold hinge are structurally controlled by the D_2 brittle-ductile deformation event. Distinct stylolitic quartz-kaolinite veins, which are limited to the ore zone and clearly associated with primary mineralization, are inconsistent with an entirely supergene origin of the argillic alteration.

Textural features including small-scale alteration halos along cracks (Fig. 6A), crystal-lined vugs within the dolomitic sandstone (Fig. 6D) and the siliceous halo around the deposit (Fig. 8H), stylolitic veins (Fig 8A) and small-scale argillic alteration halos (Fig. 8E) show unequivocally that these are hydrothermal alteration products. Geochemical changes such as K loss associated with Si, C and Mg addition fit the observed mineralogical changes superimposed on primary sedimentary variations. The observed variation within the least altered rocks are much smaller than the observed loss and gains of K, Si, C and Mg (Fig. 9), which are most likely related to the replacement of muscovite by kaolinite ± amesite and the precipitation of quartz, as observed in the carbon-rich and kaolinite-rich argillic alteration.

Reducing (amorphous carbon) and oxidizing (platy and globular hematite) alteration fronts occurred at overlapping times in the stability field of kaolinite, as recorded in fractures and primary growth zones of massive and euhedral quartz and dolomite crystals. The close concentration of high-grade Au-Pd-Pt mineralization in rocks with high carbon content indicates that preexisting carbon, as well as additional precipitated carbon that was probably advected as CH_4, acted as an essential trap for the precipitation of the precious metals as well as the suite of other redox-sensitive elements. This element suite includes Au, Pd, Pt, Bi, U, As, Se, Te and V, which are variably enriched in the primary ore at Serra Pelada. The same element suite also characterizes unconformity-related uranium deposits (Wilde et al., 1989), and particularly the low-temperature hydrothermal Au – Pd ± U deposit of Coronation Hill located in the same region as the large unconformity- related uranium deposits of Australia (Mernagh et al., 1994). These deposits are interpreted to be the product of fluid mixing between a surface-derived, deeply circulating basin brine with a reducing fluid originating from organic carbon-bearing metasediments in the basement underlying the unconformity (Wilde et al., 1989; Mernagh et al., 1994, 1998; Alexandre et al., 2005; Dérome et al., 2005; Cuney et al., 2010). We propose that the Serra Pelada deposit was localized at the site of reduction of a suite of elements that were transported in a highly oxidized fluid that had previously contacted mafic or ultramafic rocks while traversing the tectonically stacked Archean basement. Similar low-temperature hydrothermal redox processes precipitated

high-grade Au, Pd and Pt ore together with these elements by formation of minerals that are largely insoluble at reducing conditions. Such a variant of an unconformity-related redox model is a more likely explanation for the origin of Serra Pelada than a magmatic-hydrothermal process of iron-oxide-copper-gold affinity as previously proposed. An ongoing study of fluid inclusions and hydrothermal geochemistry aims at refining the proposed redox process that generated the element association and exceptional ore grades at Serra Pelada.

Acknowledgments

We gratefully acknowledge Colossus Minerals Inc. for providing data, permitting publication and financially supporting the ongoing scientific research at the deposit. GVB is thankful to all Colossus employees and the garimpeiros from Serra Pelada, for all their assistance during the time on site. We also thank Markus Wälle for help with the LA-ICPMS analysis.

References

Alexandre, P., Kyser, K., Polito, P., and Thomas, D., 2005, Alteration mineralogy and stable isotope geochemistry of Paleoproterozoic basement-hosted unconformity-type uranium deposits in the Athabasca basin, Canada: Economic Geology, v. 100, p. 1547-1563.

Almeida, F.F.M., Hasui, Y., Brito-Neves, B.B., and Fuck, R.A., 1981, Brazilian structural provinces: an introduction. Earth Science Reviews, v. 17 p. 1-29.

Avelar, V. G., Lafon, J.M., Correia, Jr. F. C., Macambira, E.M.B., 1999, O magmatismo arqueano da região de Tucumã–província mineral de Carajás: novos dados geocronológicos: Revista Brasileira de Geociências, v. 29, p. 453-460.

Barros, C.E.M., and Barbey, P., 2000, Significance of garnet-bearing metamorphic rocks in the Archean supracrustal series of the Carajás mining province, northern Brazil: Revista Brasileira de Geociências, v. 30, p. 367-370.

Berni, G.V., 2009, Geologia e alteração hidrotermal do depósito de Au-Pd-Pt de Serra Pelada, Curionópolis, Pará, Brasil: Master thesis, Universidade Federal de Minas Gerais, 116p.

Colossus Minerals Inc., 2011, Colossus Minerals drills 7.30 meters at 1494.7 g/t gold, 516.6 g/t platinum and 558.9 g/t palladium in extensions of Central Mineralized Zone at Serra Pelada, Brazil: News release. www.colossusminerals.com.

Cabral, A.R., Lehmann, B., Kwitko, R., and Cravo Costa, C.H., 2002, The Serra Pelada Au-Pd-Pt deposit, Carajás mineral province, northern brazil: reconnaissance mineralogy and chemistry of very high grade palladian gold mineralization: Economic Geology, v. 97 p. 1127-1138.

Cabral, A.R., Burgess, R., and Lehmann, B., 2011, Late Cretaceous bonanza-style metal enrichment in the Serra Pelada Au-Pd-Pt deposit, Pará, Brazil: Economic Geology, v. 106, p. 119-125.

Cuney, M., 2010, Evolution of uranium fractionation processes through time: Driving the secular variation of uranium deposit types: Economic Geology, v. 105, p. 553-569.

Derome, D., Cathelineau, M., Cuney, M., Fabre, C., Lhomme, T., 2005, Mixing of sodic and calcic brines and uranium deposition at McArthur river, Saskatchewan, Canada: A Raman and laser-induced breakdown spectroscopic study of fluid inclusions: Economic Geology, v. 100 p. 1529-1545.

Gaál, 1997, Structural geology of the Serra Pelada gold deposit in Carajás, Pará state: Internal report.

Grainger, C.J., Groves, D.I., and Costa, C.H.C., 2002, The epigenetic sediment hosted Serra Pelada Au-PGE deposit and its potential genetic association with Fe-oxide Cu-Au mineralization within the Carajás mineral province, amazon craton, Brazil: Society of Economic Geologists Special Publication 9, p. 47-64.

Grainger, C.J., 2003., The Epigenetic sediment-hosted Serra Pelada Au-PGE deposit and its potential genetic association with varying styles of Cu-Au mineralisation within the Carajás mineral province, amazon craton, Brazil. University of Western Australia, Doctoral Thesis, 259p.

Grainger, C.J., Groves, D.I., Tallarico, F.H.B., and Fletcher, I.R., 2008, Metallogenesis of the Carajás mineral province, southern amazon craton, Brazil: Varying styles of Archean through Paleoproterozoic to Neoproterozoic base- and precious-metal mineralisation: Ore Geology Reviews, v. 33, p. 451-489.

Guillong, M., Meier, D., Allan, M., Heinrich, C., and Yardley, B., 2008, SILLS: A MATLAB-based program for the reduction of laser ablation ICP-MS data of homogeneous materials and inclusions. Mineralogical Association of Canada Short Course Series, v. 40, p. 328-333.

Günther D., Frischknecht R., Heinrich C. A., and Kahlert H. J., 1997, Capabilities of an argon fluoride 193 nm excimer laser for laser ablation inductively coupled plasma mass spectrometry microanalysis of geological materials. J. Anal. At. Spectrom, v. 12, p. 939–944.

Heinrich, C.A., Pettke, T., Halter, W.E., Aigner-Torres, M., Audetat, A., Günther, D., Hattendorf, B., Bleiner, D., Guillong, M., and Horn, I., 2003, Quantitative multi-element analysis of minerals, fluid and melt inclusions by laser-ablation inductively-coupled-plasma mass-spectrometry. Geochimica et Cosmochimica Acta, v. 67, p. 3473-3497.

Jorge João, X. da S., Neves, A.P., Leal, J.W.L., 1982, Ouro da Serra Pelada, aspecto da geologia e garimpagem: Sociedade Brasileira de Geologia, Simpósio de Geologia da Amazônia, 1, Belém, v.3, p.52-61.

Nogueira, A.C.R., Truckenbrodt, W., and Pinheiro R.V.L., 1995, Formação Águas Claras, Pré-Cambriano da serra dos Carajás: redescrição e redefinição litoestratigráfica: Boletim do Museu Paraense Emílio Goeldi, n.7, p.177-197.

Neuendorf, K.K.E., Mehl, and J.P. Jackson, J.A., 2005, Glossary of Geology: American Geological Institute, Fifth edition, 779p.

Machado, N., Lindenmayer, Z., Krogh, T.E., and Lindenmayer, D., 1991, U-Pb geochronology of Archean magmatism and basement reactivation in the Carajás area, amazon shield, Brazil: Precambrian Research, v. 49, p.329-354.

Meireles, E.M.; Teixeira, J.T.; Lourenço, R.S.; and Medeiros Filho, C.A., 1982, Geologia, estrutura e mineralização aurífera de Serra Pelada: Sociedade Brasileira de Geologia, Anais do 32º Simpósio Brasileiro de Geologia, Salvador, v. 3, p. 900-911.

Meireles, E.M. and Silva, A.R.B., 1988, Depósito de Ouro de Serra Pelada, Marabá, Pará: C. Schobbenhaus & C.E.S Coelho (eds), Principais Depósitos Minerais do Brasil, Brasília, DNPM/CVRD, v. 3., p. 547-557.

Mernagh, T.P., Heinrich, C.A., Lecky, J.F., Carville, D.P., Gilbert, D.J., Valenta, R.K., and Wyborn, L.A.I., 1994, Chemistry of low-temperature hydrothermal gold, platinum and palladium (±U) mineralization at Coronation Hill, Northern Territory, Australia: Economic Geology, v.89, p.1053-1073.

Mernagh, T.P., Wyborn, L.A.I., and Jagodzinski, E.A., 1998, Unconformity-related U ± Au ± platinum group-element deposits: Australian Geological Survey Organization Journal of Australian Geology and Geophysics, v. 17, p. 197-205.

Moroni, M., Ferrario, A., and Girardi, V.A.V., 1999, Towards a model for the Serra Pelada Au-PGE deposit, Serra dos Carajás, Brazil: Stanley, C.J., et al. (eds), Processes to processing: Balkema, Rotterdam, p. 759-785.

Moroni, M., Girard, V.A.V., and Ferrario, A., 2001, The Serra Pelada Au-PGE deposit, serra dos Carajás (Pará State, Brazil): geological and geochemical indications for a composite mineralising process: Mineralium Deposita, v. 36, p. 768-785.

Pidgeon, R.T., Macambira, M.J.B., and Lafon, J.M., 2000, Th-U-Pb isotopic systems and internal structures of complex zircons from an enderbite from the Pium Complex, Carajás Province, Brazil: evidence for the ages of granulite facies metamorphism and the protolith of the enderbite: Chemical Geology, v. 166, p. 159-171.

Pinheiro, R.V.L., and Holdsworth, R.E., 2000, Evolução tectonoestratigráfica dos sistemas transcorrentes Carajás e Cinzento, Cinturão Itacaiúnas, na borda leste do Craton Amazônico, Pará. Revista Brasileira de Geociências, v. 30, p. 597-606.

Prado-Pereira, R.M., 2009, Geologia da região sul da Serra Norte e características do minério de ferro do depósito de N8, Província Mineral de Carajás: Master Thesis, Universidade Federal de Minas Gerais.131p.

Rosière, C.A., Baars, F.J., Seoane, J.C.S., Lobato, L.M., Silva, L.L., Souza, S.R.C., and Mendes, G.E., 2005, Structure and iron mineralisation of the Carajás Province: Applied Earth Science, IMM Transactions section B, n.115, p.126-133.

Tallarico, F.H.B., Coimbra, C.R., and Costa, C.H.C., 2000, The Serra Leste sediment hosted Au-(Pt-Pd) mineralization, Carajás province: Revista Brasileira de Geociências, v.30, n.2, p. 226-229.

Vasconcelos, P.M., Renne, P.R., Brimhall, G.H, and Becker, T.A., 1994, Direct dating of weathering phenomena by 40Ar/39Ar and K-Ar analysis of supergene K-Mn oxides: Geochimica et Cosmochimica Acta, v. 58, p. 1635-1665.

Villas, R.N., and Santos, M.D., 2001, Gold Deposits of Carajás Mineral Province: Deposits Types and Metallogenesis: Mineralum Deposita, v. 36, p. 300-331.

Wilde AR., Bloom MS., and Wall VJ., 1989, Transport and deposition of gold, uranium and platinum-group elements in unconformity-related uranium deposits: The geology of gold deposits: the perspective in 1988, Economic Geology Monograph 6, p. 637-650.

Wall, V.J., Berni, G.V., and Grainger, C.J., 2009, Serra Pelada, Brazil: A high-grade, hydrothermal gold-platinum-palladium system. P.J. Williams et al (eds), Proceedings of the 10th. Biennial SGA Meeting Townsville Australia 2009, p. 74-76.

FIGURE CAPTIONS

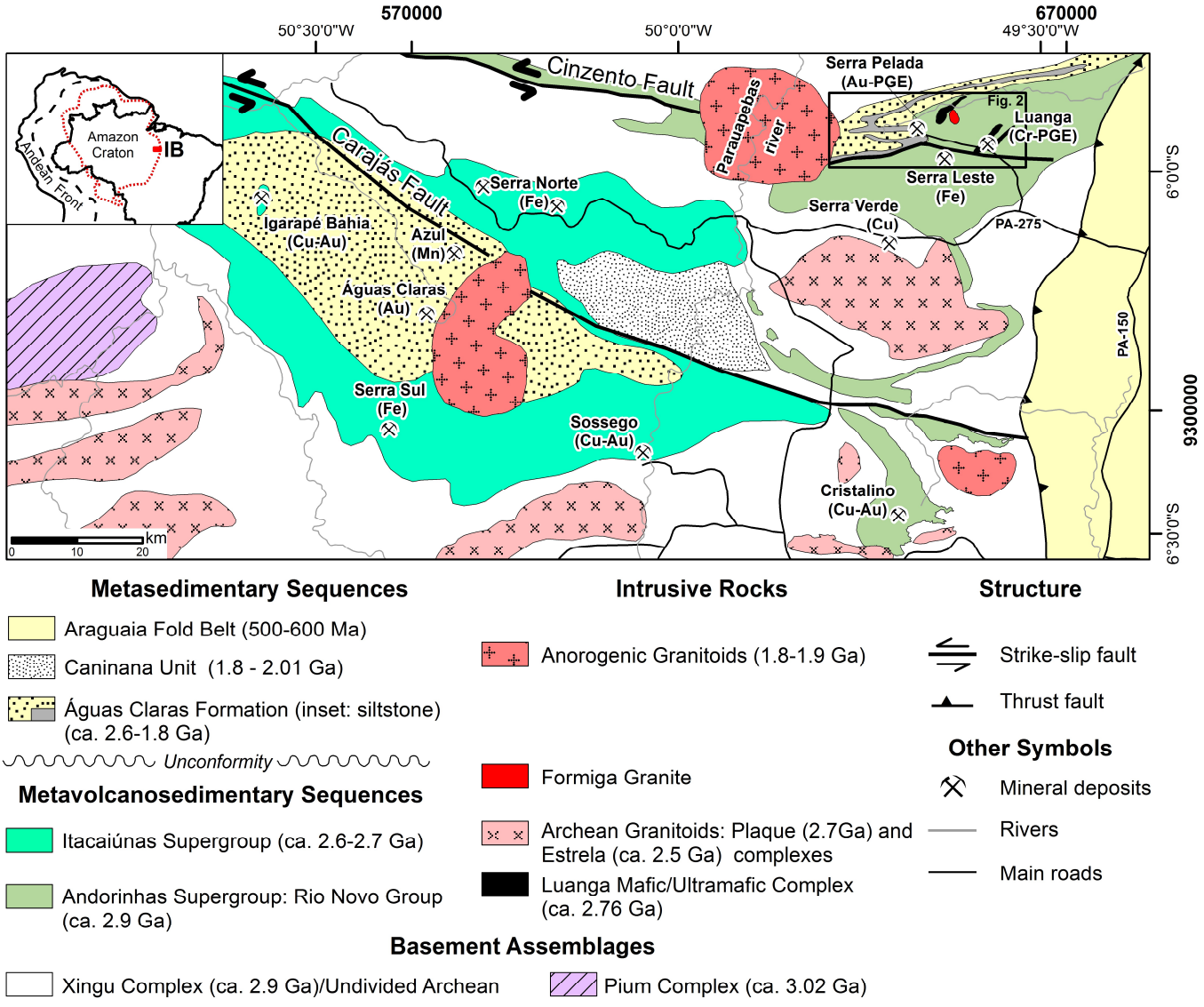

Figure 1 – Regional map of the Itacaiúnas Belt (IB - Continent-scale location on upper left; modified from Rosière et al., 2005). Ages referenced in the text. Inset shows location of Serra Pelada detailed in Figure 2.

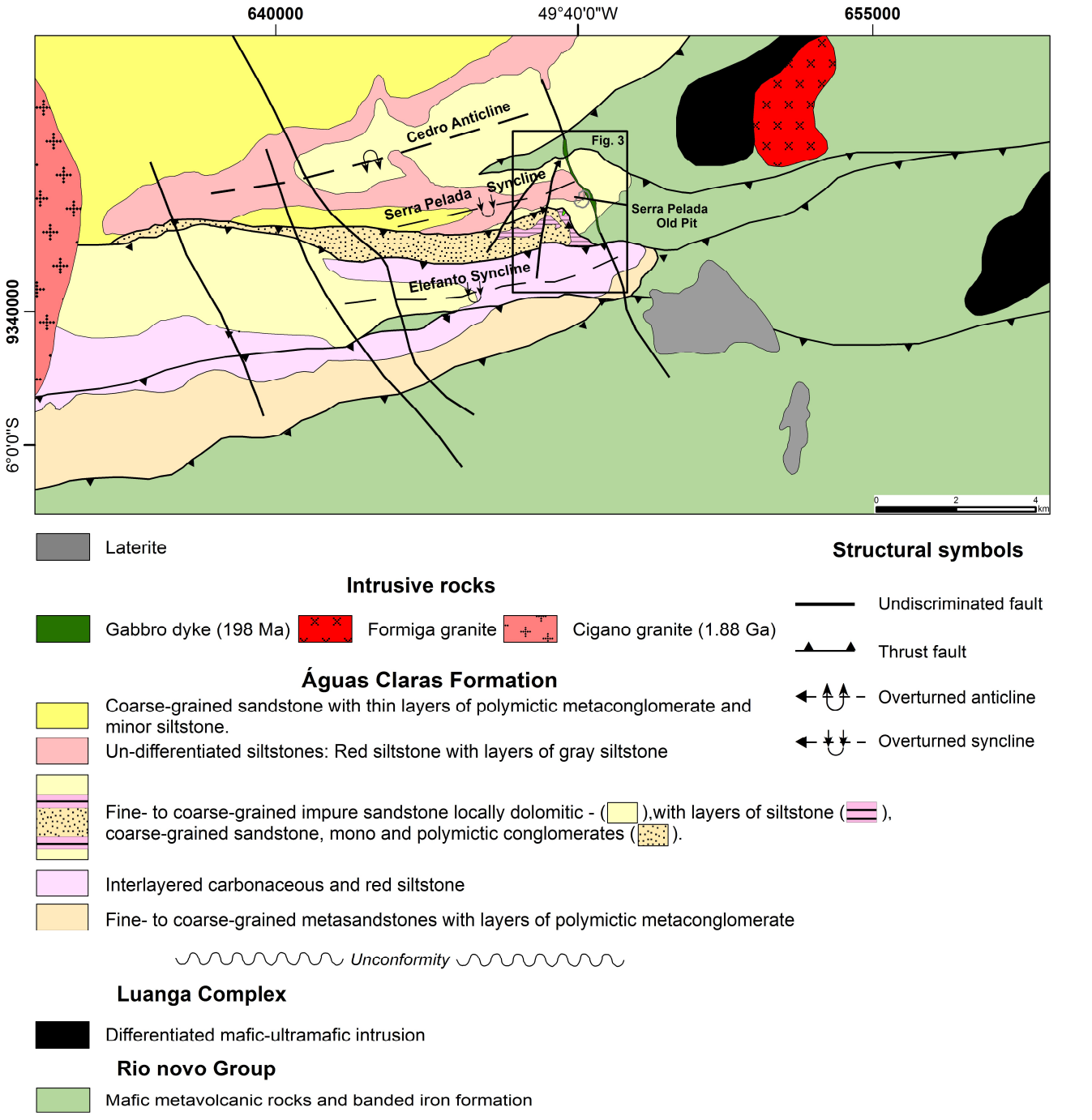

Figure 2 – District scale geological map of the Serra Pelada area (modified from Berni, 2009). Inset shows location of Serra Pelada Au – Pd – Pt deposit shown in Figure 3.

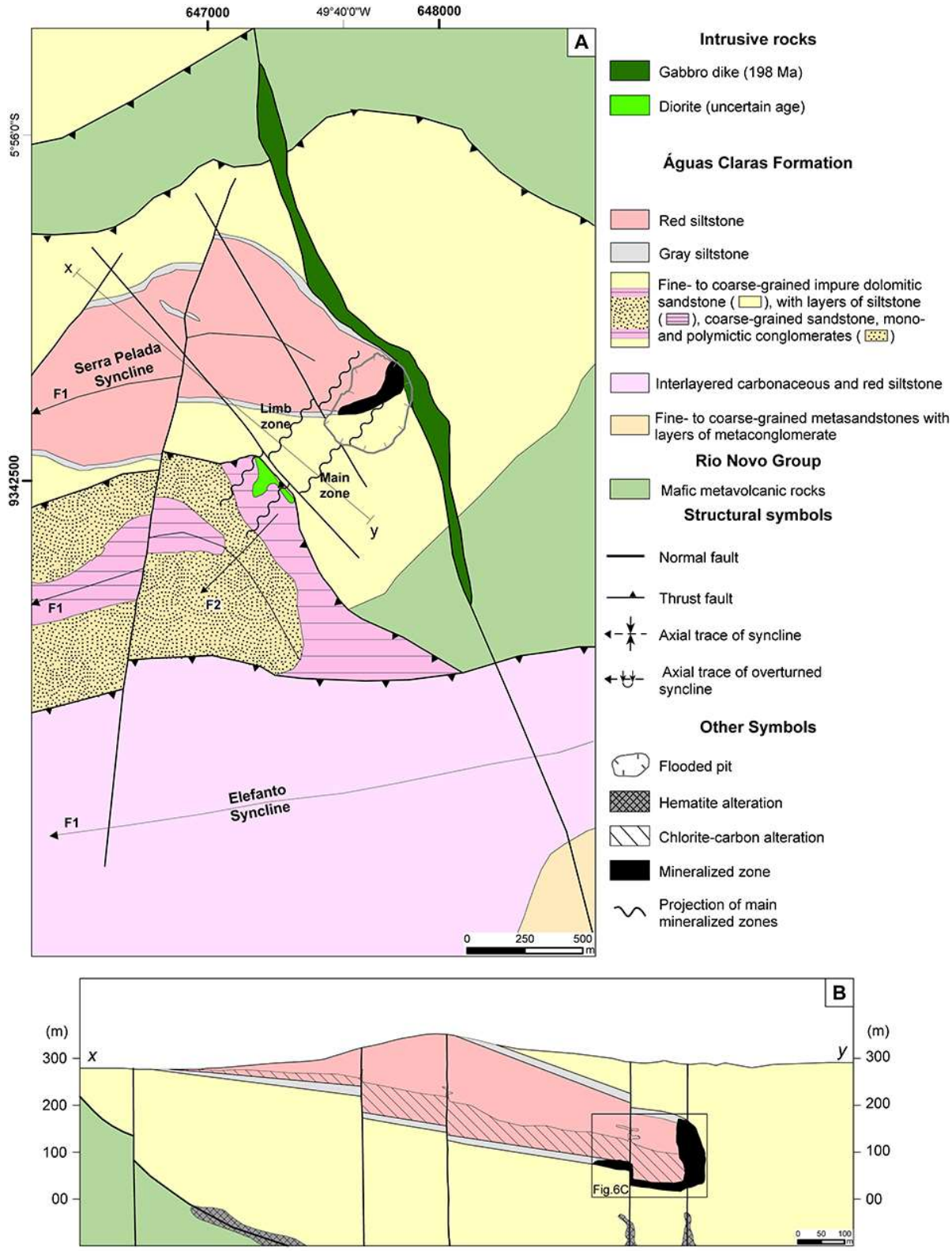

Figure 3 – Geological Map of the Serra Pelada Au – Pd – Pt deposit (modified from Berni, 2009).

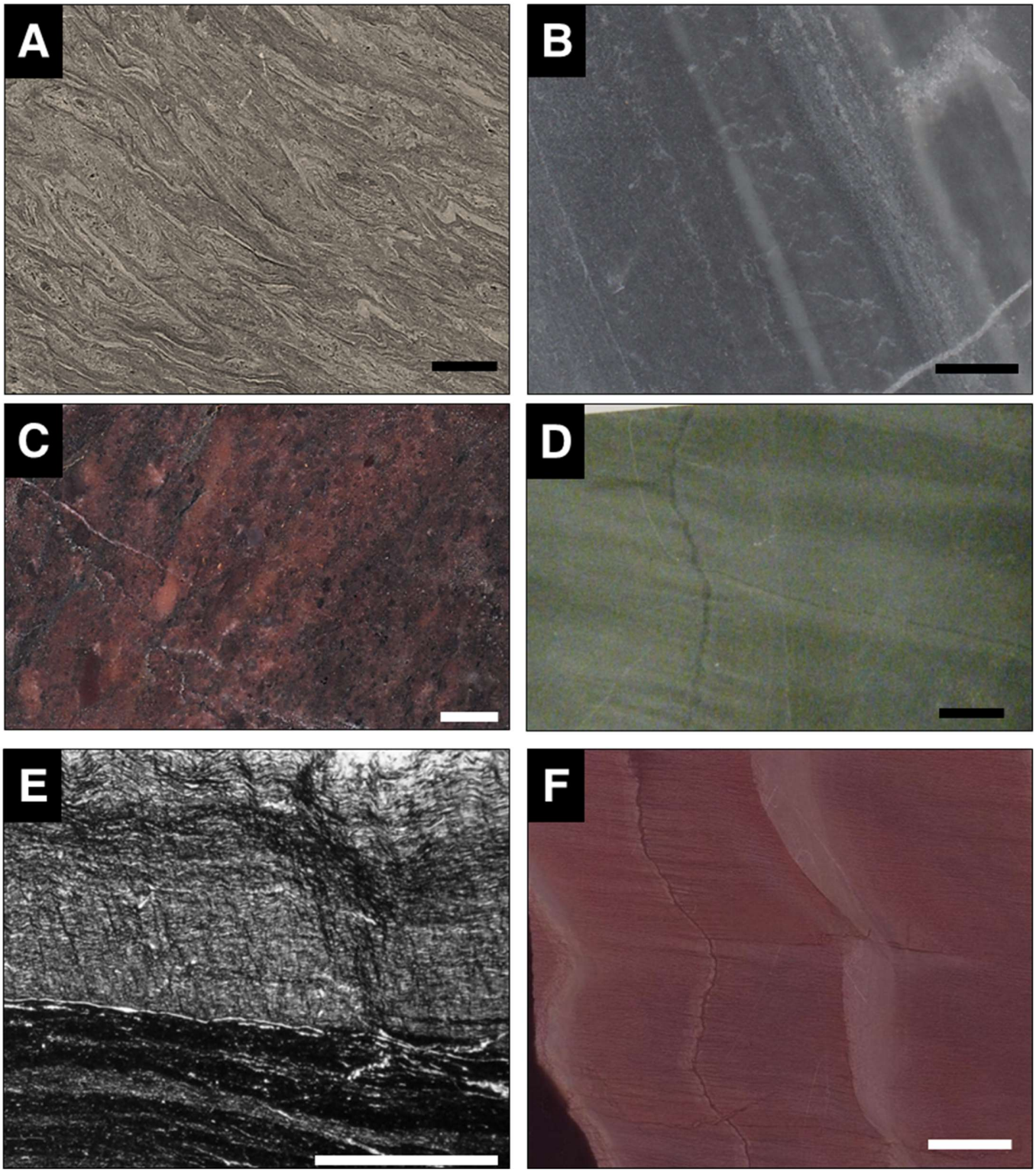

Figure 4 – Least altered rocks in and around the Serra Pelada Au – Pd – Pt deposit. (A) Chlorite-talc schist from the Rio Novo Group. (B) Fine grained dolomitic sandstone. (C) Dolomitic conglomerate with red

fragments of banded iron formation. (D) Least altered gray siltstone (<0.1 wt % C_{total}). (E) Photomicrograph of slightly altered gray siltstone showing carbon mobilization and re-precipitation along S_2 crenulation plans (subvertical structure). (F) Red siltstone with bright sandy and darker red clay-rich layers. Scale bars are 1cm.

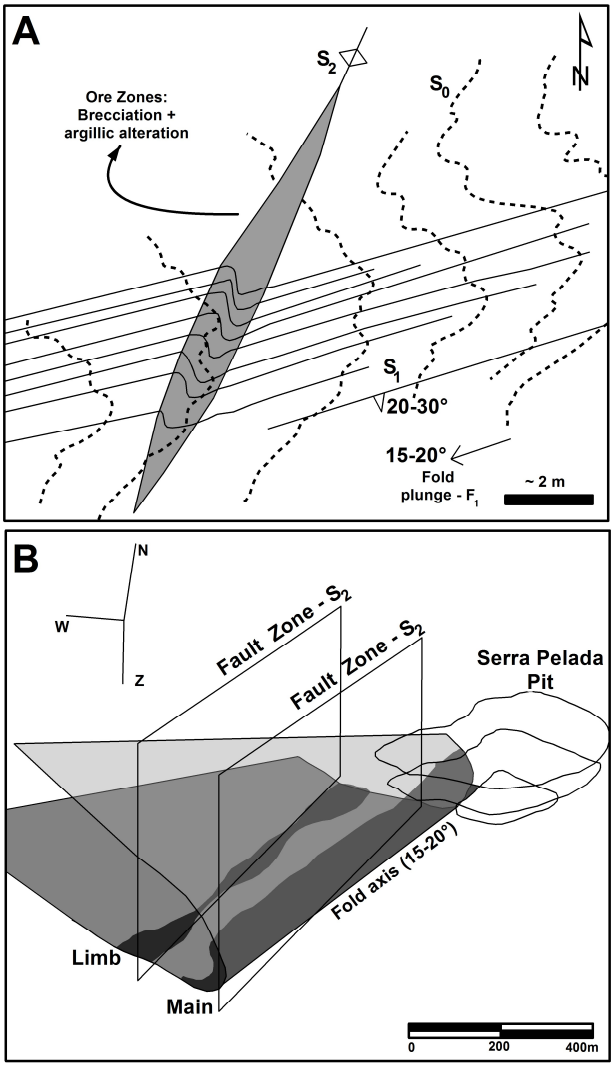

Figure 5 – Structural features of the Serra Pelada Au – Pd – Pt deposit. (A) Outcrop scale structural controls of mineralization with the main ore zone (horizontal view, after Gaál, 1997). (B) Schematic 3D view of the Serra Pelada syncline and the two ore zones of the deposit.

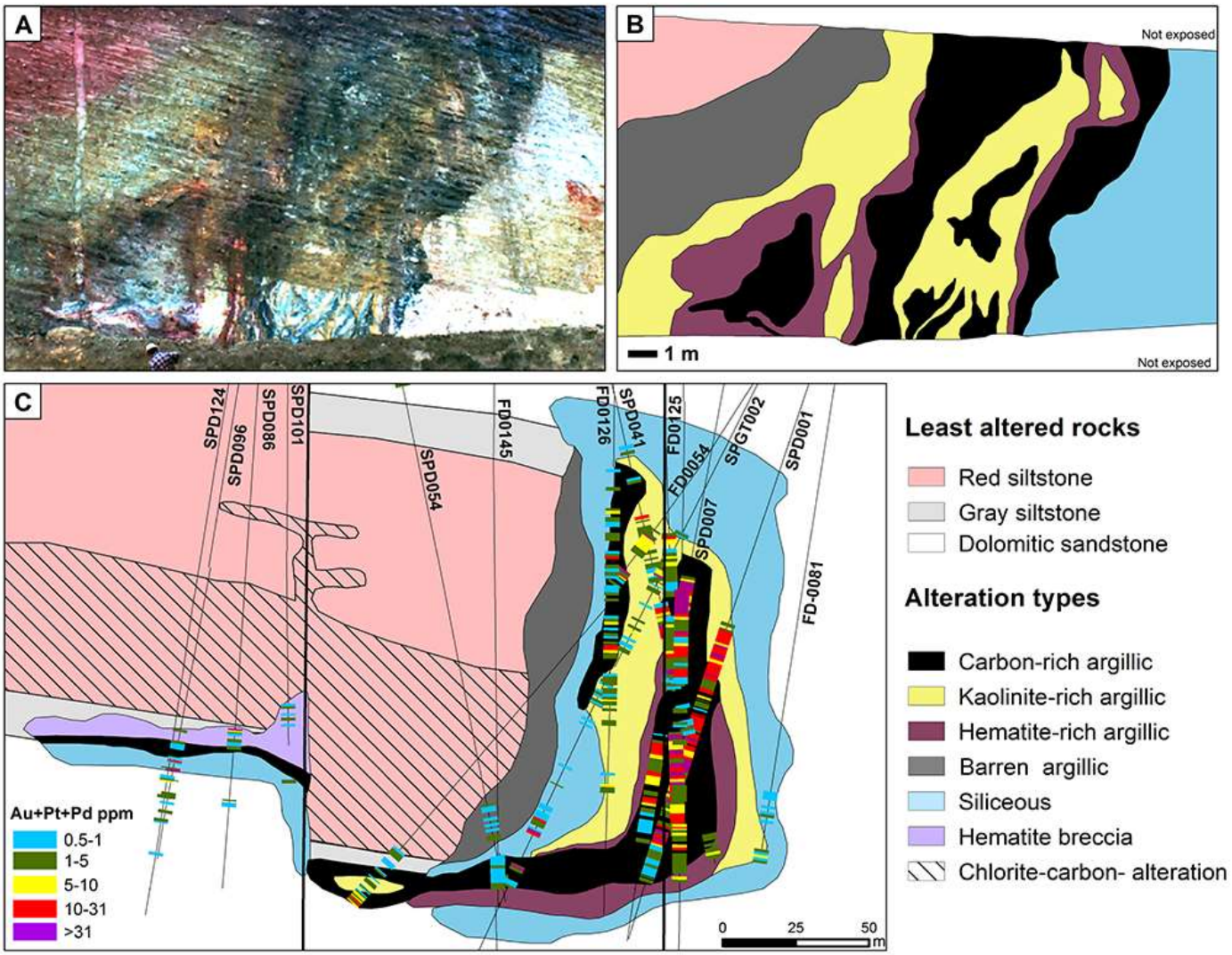

Figure 6 – (A) The possibly best photographic record of the ore zone, exposed during open-pit mining activity (note miner for scale). (B) Interpretation of the alteration zones within the photograph in A. (C) Geological cross section (see Fig. 3 for location) with alteration zones and Au + Pt + Pd grades along exploration drill cores, constructed from recent exploration data.

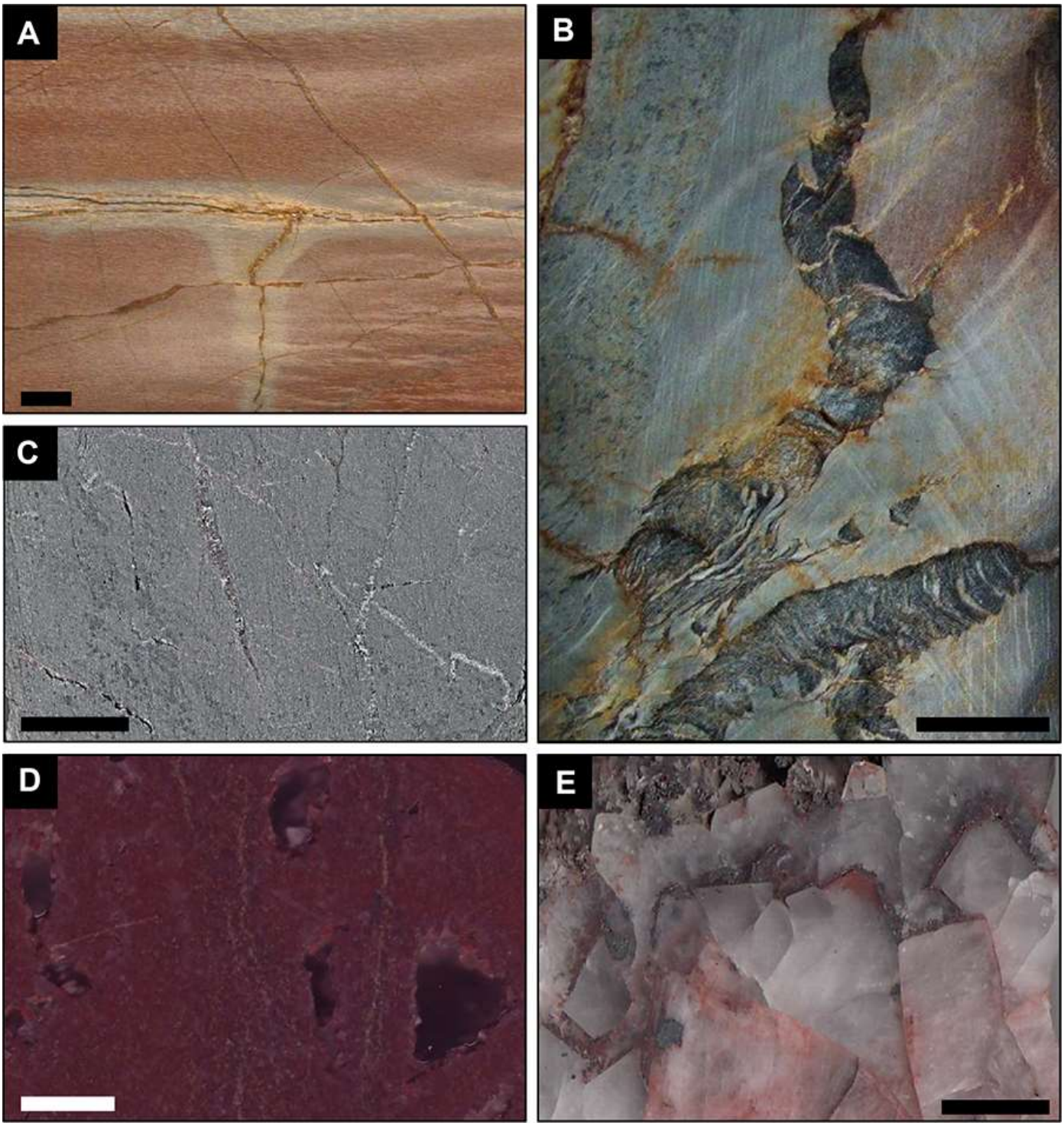

Figure 7 – Distal alteration zones around the Serra Pelada Au – Pd – Pt deposit. (A) Chlorite + carbon alteration at subvertical crack, extending along compositional layering of the red siltstone. (B) Carbon-quartz veins within chlorite altered red siltstone. (C) S_2 oriented chlorite totally overprinting red siltstone. (D) Coarse-

grained, hematite-altered dolomitic sandstone with dissolution vugs lined by hematite-dusted dolomite. (E) Detail of vug with co-precipitated crystals of quartz, dolomite and hematite, from large fracture zone cutting through the rocks shown in D; growth zones in crystals are lines with fine-grained sulfides enriched in Ni, Pt and other ore-related elements. Scale bars are 1cm.

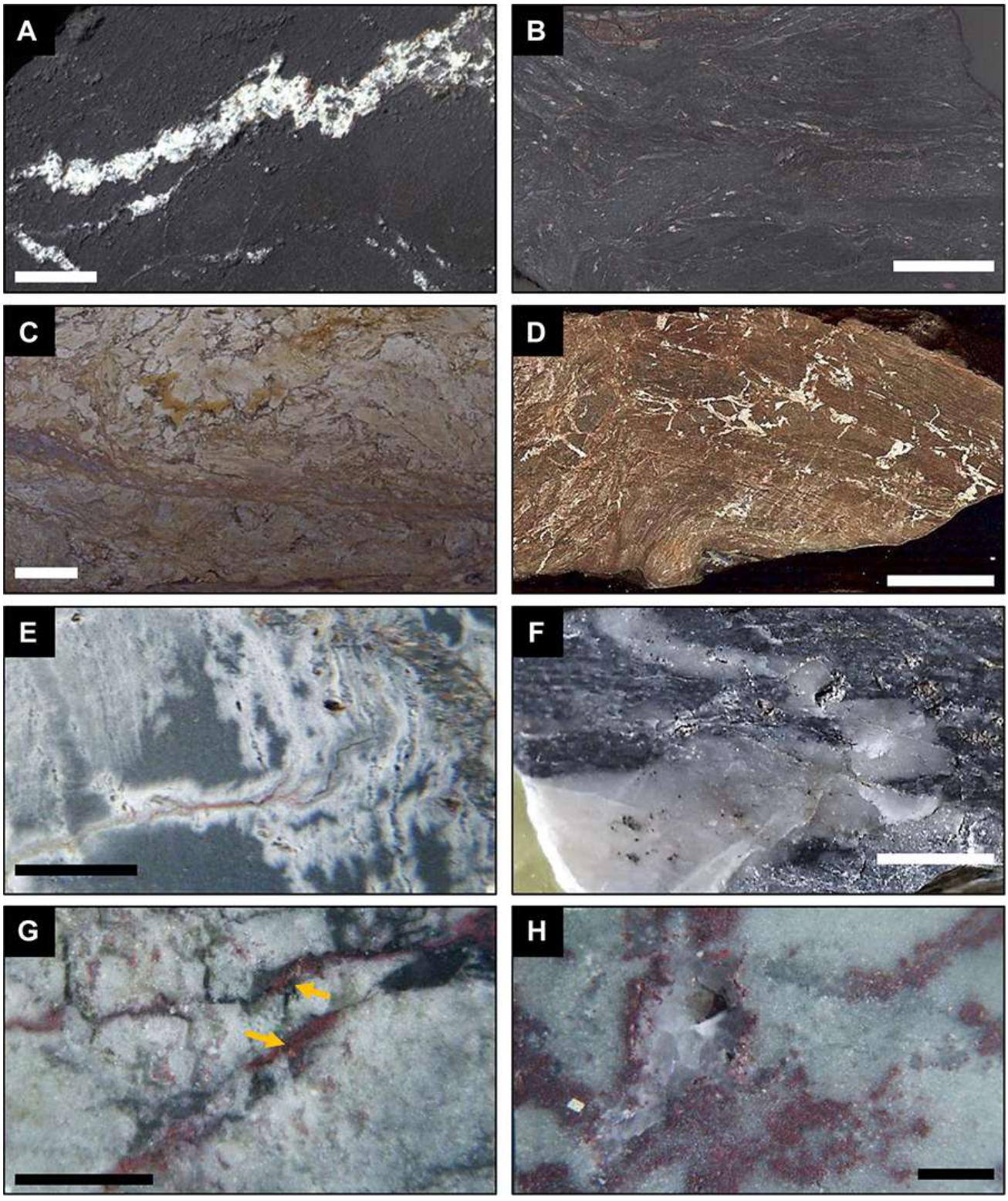

Figure 8 – Alteration types from deep near-vertical drill holes intersecting the ore zone. (A) Coherent carbon-enriched siltstone with stylolitic quartz - kaolinite vein containing gold, fischesserite with minor primary

hydrothermal sulfides including Se-covellite and chalcopyrite. (B) High grade carbonaceous breccia (~ 640 ppm Au, 360 ppm Pd, 255 ppm Pt). (C) Kaolinite-rich argillic alteration. (D) Hematite-rich argillic alteration, weakly gold-mineralized. (E) Barren sericite alteration extending vertical along S_2 crenulation. (F) Deformed pre-ore quartz vein showing that at least some silicification predated or was coeval with the S_1 axial plane foliation. (G) Fine-grained later siliceous alteration showing near-coeval carbon and hematite veinlets. (H) Fine-grained siliceous alteration with vugs partly filled by coarse quartz, with globular and platy hematite at the base and along growth zones of the euhedral crystals. All scale bars are 1cm.

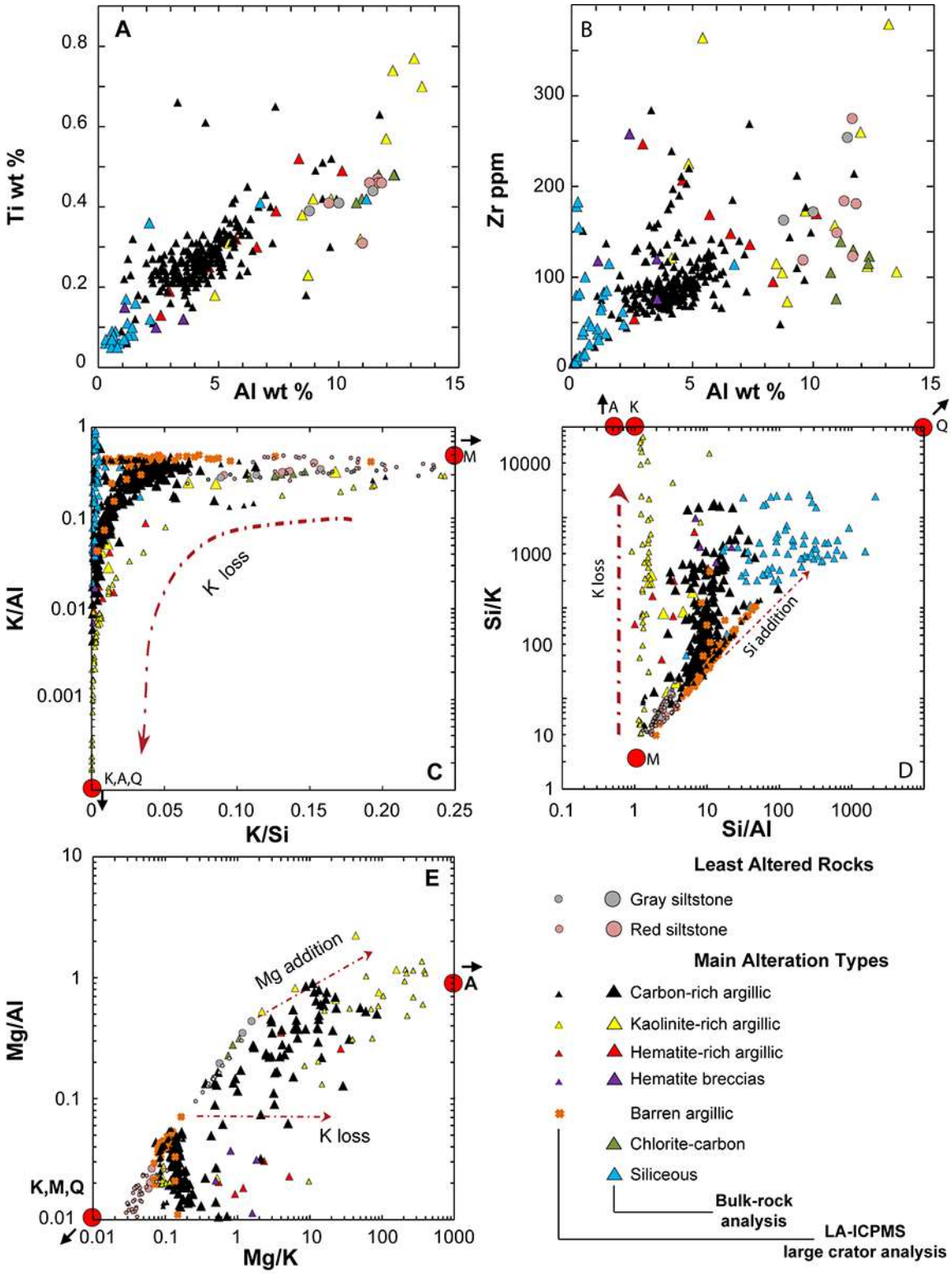

Figure 9 – Bulk-rock concentrations of Ti, Al and Zr, as a selection of relatively immobile elements maintaining approximately constant ratios during hydrothermal silicification, hematite and/or carbon addition

(A, B). Ratio plots (C, D and E) comparing selected major elements proportions for least altered rocks and main alteration types within the Serra Pelada Au – Pd – Pt deposit, showing K-loss during ore-related kaolinitization, silicification and Mg-alteration. Big symbols are whole rock, small symbols are LA-ICPMS analyses. Red circles represent the stoichiometric compositions of minerals: M = muscovite; K = kaolinite; A = Amesite; Q = Quartz.

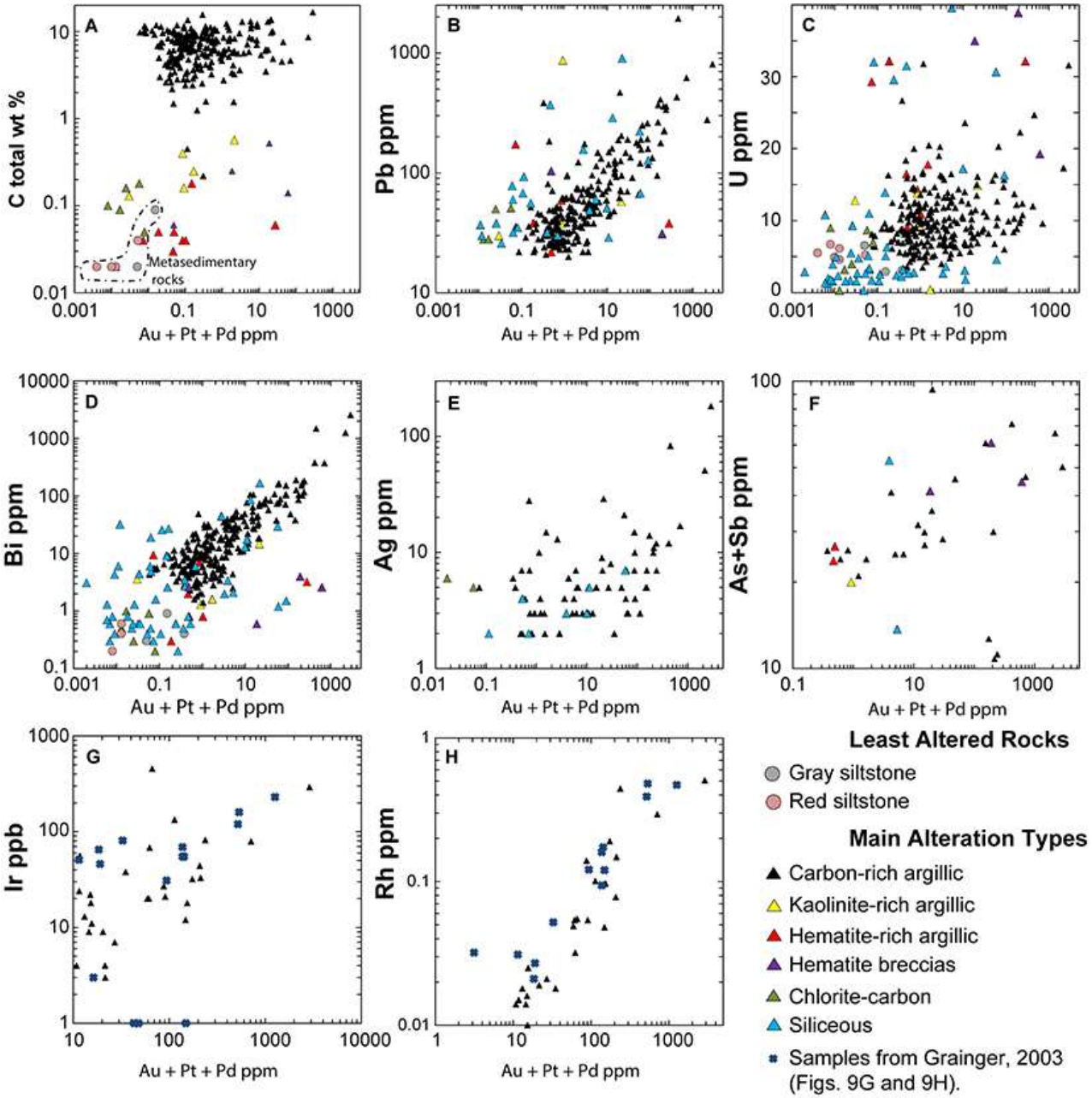

Figure 10 – Variation diagrams for carbon and selected ore-related trace elements as a function of total Au + Pd + Pt ore grade, comparing the least altered rocks with main alteration types within the Serra Pelada deposit. Note that that high-grade ores contain orders of magnitude more C_{total} than reduced country rocks, with a correlation between precious metal grades and concentrations of Pb, U, Bi, Ag, As + Sb and (at very low levels) Ir and Rh.

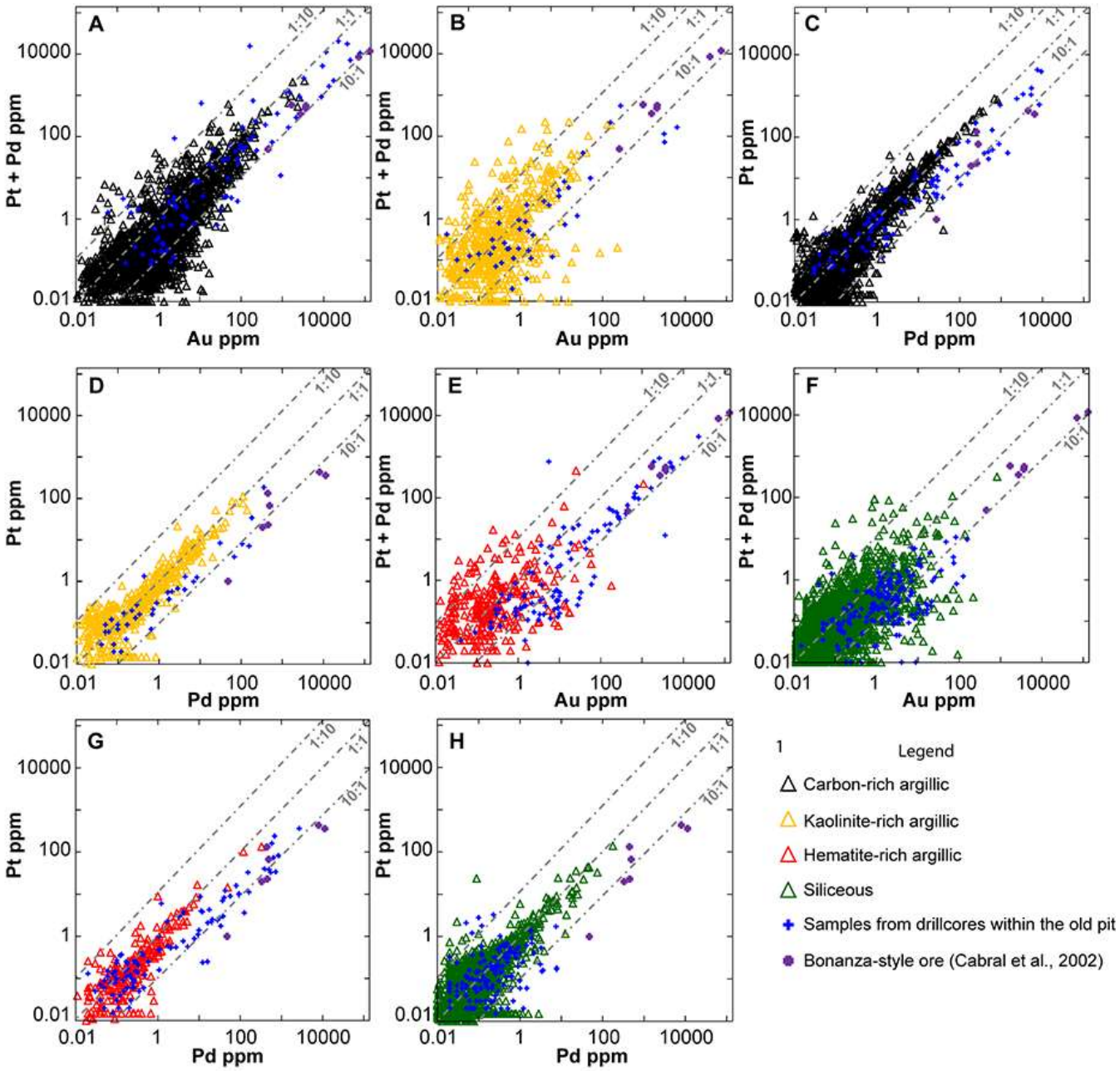

Figure 11 – Metal concentrations grouped according to different ore types in the Serra Pelada deposit, linked with logging information from more than 60,000 m of diamond drill core (data obtained by Colossus Minerals

Inc. from all drilling campaigns between 1980's to 2008). Note that near-surface samples that are largely oxidized to Fe- and Mn-oxy-hydroxides (from Cabral et al., 2002) are most extremely enriched in precious metals, with depletion of Pt relative to Au and Pd.

DIGITAL REPOSITORY

Table 1 – Major and trace element composition for least altered rocks and main hydrothermal alteration types at Serra Pelada Au – Pd – Pt deposit.

Table 2 – Bulk-rock major element ratios from LA-ICPMS analysis of 110 μm ablation pits.